Available online at www.sciencedirect.com
ScienceDirect
Journal of Nuclear Materials 363–365 (2007) 1206–1210
journal of nuclear materials
www.elsevier.com/locate/jnucmat

Theoretical and experimental characterization of damaged graphite surfaces

Y. Ferro [a,*], C. Thomas [c], T. Angot [c], P. Génésio [b], A. Allouche [a]

[a] *Laboratoire de Physique des Interactions Ioniques et Moléculaires, Université de Provence et CNRS – UMR 6633, Campus de Saint Jérôme, Services 242, 13397 Marseille cedex 20, France*
[b] *Laboratoire de Physique des Interactions Ioniques et Moléculaires, Université de Provence et CNRS – UMR 6633, Campus de Saint Jérôme, Services 232, 13397 Marseille cedex 20, France*
[c] *Laboratoire de Physique des Interactions Ioniques et Moléculaires, Université de Provence et CNRS – UMR 6633, Campus de Saint Jérôme, Services 241, 13397 Marseille cedex 20, France*

Abstract

We modeled damaged-irradiated carbon plasma facing component PFCs by graphite surfaces with vacancies. We combined theoretical and experimental investigations with a view to building tools to make a better assignment of the observed defects from the scanning tunneling microscope (STM) images. The theoretical part of this work is based on periodic density functional theory calculations. The electronic structure is calculated and the density of state along with the electronic density near the Fermi level are plotted. STM images are further simulated and their features are interpreted. On the experimental side, we performed scanning tunneling microscopy (STM) imaging at low bias voltage in order to probe the electronic modifications of the graphite surface induced either by H^+ (or D^+) ion bombardment and/or atomic H (respectively D) adsorption. A connection between STM images and the reactivity of defective graphite surfaces towards H is also proposed.

PACS: 71.15.Mb; 68.37.Ef; 81.05.Uw

Keywords: Graphite; Spectroscopy; Defects

1. Introduction

Plasma–material interaction remains one of the crucial issues for the deuterium–tritium thermonuclear fusion reactor development. Because of their low atomic number and high thermal shock resistance, carbon-based materials are currently used in tokamaks to protect the plasma facing components (PFCs). Thus, carbon fiber composites will be used to handle high-heat fluxes incident on the divertor plates in the next magnetically-controlled fusion device ITER [1]. PFCs undergo physical and chemical erosion during shots. There results a strong modification in their structures and morphologies. Scanning tunneling microscopy (STM) is one of the techniques which allow investigating graphite defective surfaces. STM topography is a map of constant charge density at the Fermi level (ρ_{STM}). Thus, the interpretation of images is not

* Corresponding author.
E-mail address: yves.ferro@up.univ-mrs.fr (Y. Ferro).

0022-3115/$ - see front matter
doi:10.1016/j.jnucmat.2007.01.254

straightforward and requires a good knowledge of the electronic properties of the surface [2]. Defects created by the impinging particle fluxes on the carbon surfaces also induce a modification in the hydrogen retention yield and diffusion properties. These changes in reactivity were recently studied with an atomic vacancy [3] and a boron atom [4] as defects. While boron maintains the in-plane σ system, it behaves like an atomic vacancy for the π system by introducing an electronic hole.

In this paper, we studied the electronic properties of a graphite surface with vacancies by means of density functional theory (DFT) calculations. The understanding of the electronic properties of the graphite surface with vacancies is a tool for the interpretation of STM images. We believe these properties to be similar for surfaces with vacancies and with boron atoms. We also attempted to make a connection between the high-electronic density region as probed by STM near the vacancy and the high reactivity of the surface towards H atoms near boron atoms.

2. Method of calculation and experimental details

Calculations were performed in the DFT framework using the Perdew, Burke and Ernzerhof GGA functional for exchange and correlation [5] as implemented in the ABINIT package [6]. The core-valence electron interactions were modeled by means of the Trouiller–Martins pseudopotentials [7] and a plane-waves basis set was used with an energy cutoff of 25 Hartrees. The working cell is a reconstruction of an $n \times n$ surface unit cell of one layer in thickness, each slab being separated by a vacuum of 10 Å. The Brillouin Zones associated with each working cell were sampled in order to get an equivalent $36 \times 36 \times 1$ $\boldsymbol{k}$ points mesh for the Brillouin zone associated to the unit cell.

Experiments were performed in a series of interconnected ultra-high vacuum chambers. HOPG graphite (ZYA grade) was cleaved in air with adhesive tape, and annealed at 600 °C under vacuum for 1 h. The surface was bombarded at room temperature with 10^{13} H^+ ions/cm^2 of 300 eV energy before being imaged by STM (VT-STM, Omicron).

3. Choice of a suitable model for graphite

Defects on graphite surfaces induce long-range perturbations and act as scattering centers on the electronic wave functions [8]. STM probes the electronic density near the Fermi level (ρ_{STM}) in the narrow region [$E_{Fermi}+V_{bias}$; E_{Fermi}] where V_{bias} is the bias voltage applied on the tip. ρ_{STM} is made of all square modulus of the one-electron wave functions $|\phi_{\mathbf{k},i}|^2$ whose eigenvalues belong to this domain of energy. They are characterized by a wave vector close in both direction and norm to the one at the Fermi level: $\mathbf{k}_f$. The associated wavelength $\boldsymbol{\lambda}_\mathbf{f}$ is $3a/2$, where $a = 2.45$ Å is the unit-cell parameter of the hexagonal surface cell. Charge density waves (CDW) with a wavelength $\lambda = 3a$ are thus observed in the vicinity of the defect and form a $(\sqrt{3} \times \sqrt{3})$ R30° superstructure [8].

Because of this long-range perturbation and of the computational capability, it is impossible to choose a working cell large enough for these defects not to interact from cell to cell. This problem was addressed by choosing a working cell whose parameters are $3n \times 3n$ that of the surface unit cell. This choice allows not destroying the CDW formed by one defect inside the working cell.

4. Defective graphite surfaces

4.1. The atomic vacancy

In Fig. 1, we plotted the density of state (DOS) for a perfect layer of graphite and for the 3×3, 6×6 and 9×9 working cells with an atom vacancy in their centers. Thus, those models are increasingly more diluted in defect surface concentration. In each case and for easier comparison, the Fermi level was shifted to 0 eV. The structure of the DOS for the most diluted system is close to that of graphite. However, some localized states appear at the Fermi level, in the energy domain belonging to that of STM. The peak associated to the defect grows in intensity with defects concentration. At the same time the rest of the DOS deviates from that of a perfect graphite layer. The DOS of the 3×3 system is really damaged in each of the σ and π domains and does not resemble to that of graphite anymore.

In Fig. 2(a) we plotted ρ_{STM} for the 6×6 working cell. This plot is based on the summation over all states below the Fermi level and belonging to the [$E_{Fermi} + V_{bias}$; E_{Fermi}] domain of energy (where $V_{bias} = -360$ mV). This is an approximate way of simulating STM images, the main approximation being (i) that the tunneling matrix element is supposed to be independent of the lateral tip position and of the bias voltage and (ii) that the tip state is described by a locally spherical potential.

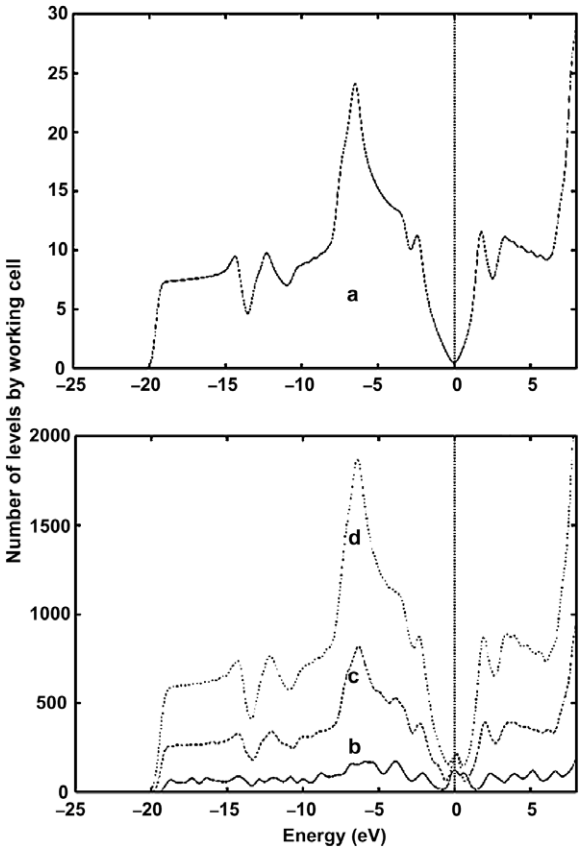

Fig. 1. Density of state for (a) a perfect graphite slab and for (b) 3×3 (c) 6×6 and (d) 9×9 working cells.

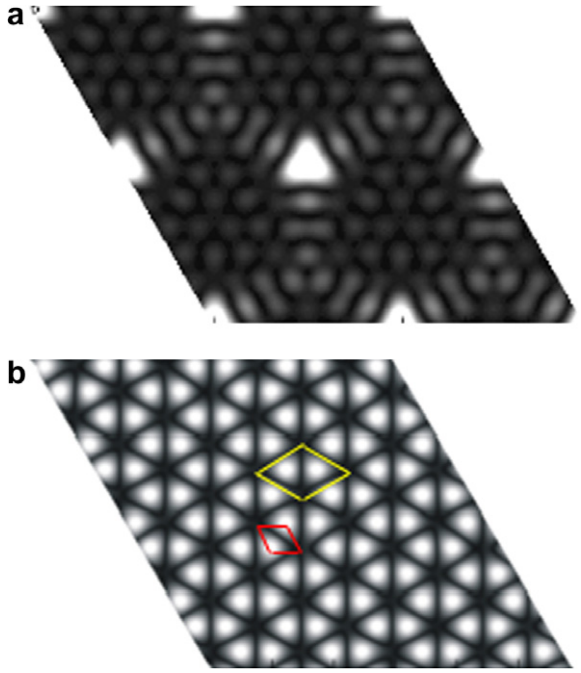

Fig. 2. Computer simulation of an STM image due to carbon atom vacancy of type A. (a) For a bias voltage of −360 mV. The grey level intensity corresponds to the tunneling current for a tip scanning at constant height (3.0 Å). (b) Calculated spatial map of a single $|\phi_{k,i}|^2$ belonging to ρ_{STM} exhibiting the $(\sqrt{3}\times\sqrt{3})$ R30° superstructure. $\phi_{k,i}$ is a linear combination of $2p_{z_A}$ orbital.

We observe a threefold symmetry structure. This symmetry is in line with that of the defect. ρ_{STM} rapidly decreases from the center of the defect to the border of the working cell. The surface unit cell of graphite contains two carbon atoms we label A and B. Let us assume we have removed an A atom to create the vacancy. In the background of the image in Fig. 2(a) we observe that ρ_{STM} is only carried by B-type atoms and no B type not A-type.

The $(\sqrt{3}\times\sqrt{3})$ R30° superstructure does not appear in Fig. 2(a). We analyzed the structure of all the wave functions involved in ρ_{STM}. At the $\overline{\Gamma}$ point of the 2 D Brillouin zone we found two contributions: linear combinations of $2p_{z_B}$ orbital (the anti-symmetric one is shown in Fig. 2(b)), and one linear combination of $2p_{z_A}$ with a node on the vacancy in order to satisfy the reflection requirement on the defect. These contributions all exhibit the $(\sqrt{3}\times\sqrt{3})$ R30° superstructure which is fully delocalized on the whole surface. These contributions are masked by the rest of those belonging to ρ_{STM}, from which arises the three-order feature. However, their intensities do not decrease in relation to distance from the defect. A more detailed analysis of the electronic structure of defective graphite surface is given in Ref. [9].

4.2. STM results

A typical STM image of an H^+ bombarded graphite surface, under the experimental conditions described in Section 2, is presented in Fig. 3. Defects always appear as bright protrusions. They clearly induce long-range (circa 5 nm) perturbations of the electronic density with a marked $(\sqrt{3}\times\sqrt{3})$ R30°. We used similar imaging when the graphite surface was exposed to atomic hydrogen fluxes [10] and such a behavior was also reported in the case of hydrogen–plasma exposed surfaces [11]. Undamaged zones away from the defect reflect the threefold symmetry of the graphite surface unit cell because only one out of two atoms is imaged [2].

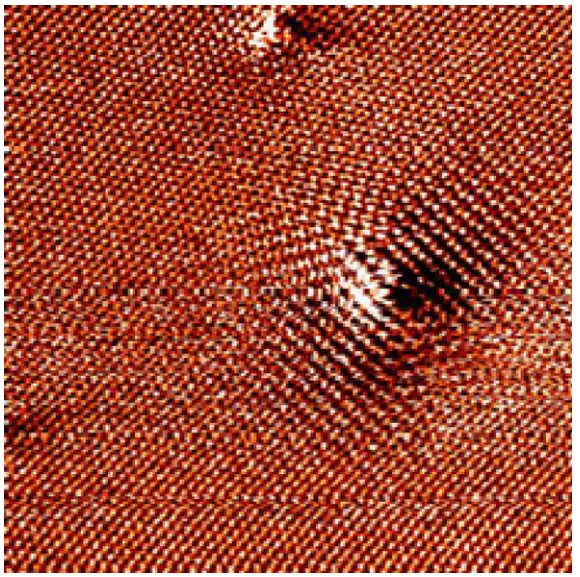

Fig. 3. 15 nm × 15 nm STM image (bias voltage 70 meV) of isolated defects.

5. Discussion and conclusion

From the choice of the working cell we made, we determined two major contributions driving the main features of STM images of defective graphite surfaces.

One of the two is a localized perturbation from two points of view: it is localized on the DOS at the Fermi level in a domain of energy that is relevant for STM, and it is localized in space since the associated density decreases in intensity from the center of the defect. This component exhibits the three-fold symmetry feature.

The other contribution is absolutely delocalized on the whole surface and also exists in pure graphite. The wave functions of this contribution may be written as two linear combinations of atomic orbital centered on the A and B atoms

$$\varphi_{i,\vec{k}\mathrm{f}}(\bar{r}) = \frac{1}{\sqrt{V}} \sum_{\vec{R}} 2\mathrm{p}_Z^{\alpha}(\vec{r} - \vec{R}) \exp(\mathrm{i}\vec{k}_\mathrm{f} \cdot \vec{R}) \quad \alpha = \mathrm{A}, \mathrm{B}. \tag{1}$$

At the Fermi level, these linear combinations are eigenstates of the one-electron Hamiltonian at the $\overline{K}$ point of the Brillouin zone. With a defect on an A-type atom, symmetric combinations of $\exp(\mathrm{i}\vec{k}_\mathrm{f} \cdot \vec{R})$ and $\exp(-\mathrm{i}\vec{k}_\mathrm{f} \cdot \vec{R})$ are forbidden for $2\mathrm{p}_Z^{\mathrm{A}}$, while antisymmetric combinations, with a node on the defect, along with the linear combinations on $2\mathrm{p}_Z^{\mathrm{B}}$ are not affected by the perturbation.

Thus, the whole electronic structure near the Fermi level consists of one component due to the defect and vanishes at a long distance away from it, and of another component which is the remaining part of the electronic structure of perfect graphite that had not been affected by the defect. The size of the working cell, however, is too small to allow the first contribution to vanish and consequently the $(\sqrt{3} \times \sqrt{3})$ R30° superstructure never appears because of lesser intensity although its existence has been demonstrated and should appear at a longer distance from the defect.

From the experimental point of view, as mentioned before, the strong increase of the local density of state results in bright imaging protrusions at the location of the defects. According to their 300 eV incident kinetic energy, it is generally expected that H^+ ions, as they penetrate by a few nanometers into the graphite, will eventually generate on their path one or more defects of different kinds. As STM probes the very last surface plane, it may not be very sensitive to strongly buried defects, nor permit any discrimination between vacancies and interstitial defects. In any case, as far as the present observations are concerned, the majority of protrusions do feature the threefold symmetry in agreement with our model calculation of vacancies. The intensity is relatively localized, but nevertheless extends over a few nanometers, as does the $(\sqrt{3} \times \sqrt{3})$ R30° superstructure, clearly identified in direct imaging as well as in Fourier transform.

From Fig. 2(a), we observe that ρ_{STM} is high on the first and third nearest neighbor of the vacancy, while it is not on the second neighbor. We have shown in a previous work [12] with a boron atom as defect that the reactivity towards H atoms behaves in a similar fashion: it is high on the first and third nearest neighbors and low on the second one. We have also shown in this work that these are levels near the Fermi level which are involved in the bonding with H. Thus, the STM image may be seen as a map of the reactivity of the surface towards H.

Boron ($2\mathrm{s}^2\ 2\mathrm{p}^1$) gets one electron less than carbon ($2\mathrm{s}^2\ 2\mathrm{p}^2$). The local DOS near the Fermi level involves only π type levels. Filling a carbon vacancy with a boron atom restores the in-plane σ system and not the π system where an electronic hole still remains. Boron differs from carbon by its atomic

charge and, as the vacancy, it acts as a scattering center for the electronic π wave. We expect the same pattern for the STM image of boron and vacancy in graphite; this would be in good agreement with the reactivity of the boron-doped surface towards H.

Finally, the simulations we ran on the basis of DFT calculations are in fairly good agreement with experimental observations as seen in Fig. 3, since the $(\sqrt{3}\times\sqrt{3})$ R30° modulation of ρ_{STM} is well reproduced. Calculations on double vacancies are in progress to verify the loss of the three-order symmetry we postulated. Calculations are also in progress on H-adsorbed surface and boron-doped graphite in order to provide tools for the interpretation of STM images and facilitate their interpretation.

Acknowledgements

We would like to thank J.-P. Legré for our constructive discussions. This work is supported by the Euratom-CEA association in the framework of the LRC (Laboratoire de Recherche Conventionnée CEA/DSM – Université de Provence PIIM).

References

[1] G. Federici et al., J. Nucl. Mater. 313 (2003) 11.
[2] D. Tomanek et al., Phys. Rev. B 35 (1987) 7790.
[3] A. Allouche, Y. Ferro, Carbon 44 (2006) 3320.
[4] Y. Ferro, A. Jelea, F. Marinelli, A. Allouche, J. Chem. Phys. 120 (2004) 11882.
[5] J.P. Perdew, K. Burke, M. Ernzerhof, Phys. Rev. Lett. 77 (1996) 3865.
[6] Available from: <http://www.abinit.org>.
[7] N.K. Trouiller, J.L. Martins, Phys. Rev. B 43 (1991) 1993.
[8] H.A. Mizes, J.S. Foster, Science 244 (1989) 559.
[9] Y. Ferro, A. Allouche, in press.
[10] C. Thomas, T. Angot, in press.
[11] P. Ruffieux, M. Melle-Franco, O. Gröning, M. Bielmann, F. Zerbetto, P. Gröning, Phys. Rev. B 71 (2005) 153403.
[12] Y. Ferro, F. Marinelli, A. Allouche, J. Chem. Phys. 118 (2003) 5650.